

A Coincidence Search for Cosmic Neutrino and Gamma-Ray Emitting Sources Using IceCube and Fermi-LAT Public Data

C. F. Turley^{1,2}, D. B. Fox^{2,3,4}, A. Keivani^{1,2}, J. J. DeLaunay^{1,2}, D. F. Cowen^{1,2,3}, M. Mostafá^{1,2,3}, H. A. Ayala Solares^{1,2}, and K. Murase^{1,2,3}

¹ Department of Physics, Pennsylvania State University, University Park, PA 16802, USA; cft114@psu.edu

Abstract

We present results of an archival coincidence analysis between Fermi Large Area Telescope (LAT) gamma-ray data and public neutrino data from the IceCube neutrino observatory's 40-string (IC 40) and 59-string (IC 59) observing runs. Our analysis has the potential to detect either a statistical excess of neutrino + gamma-ray $(\nu + \gamma)$ emitting transients or, alternatively, individual high gamma-multiplicity events, as might be produced by a neutrino observed by IceCube coinciding with a LAT-detected gamma-ray burst. Dividing the neutrino data into three data sets by hemisphere (IC 40, IC 59-North, and IC 59-South), we construct uncorrelated null distributions by Monte Carlo scrambling of the neutrino data sets. We carry out signal-injection studies against these null distributions, demonstrating sensitivity to individual $\nu + \gamma$ events of sufficient gamma-ray multiplicity, and to $\nu + \gamma$ transient populations responsible for >13% (IC 40), >9% (IC 59-North), or >8% (IC 59-South) of the gamma-coincident neutrinos observed in these data sets, respectively. Analyzing the unscrambled neutrino data, we identify no individual high-significance neutrino + high gamma-multiplicity events and no significant deviations from the test statistic null distributions. However, we observe a similar and unexpected pattern in the IC 59-North and IC 59-South residual distributions that we conclude reflects a possible correlation (p = 7.0%) between IC 59 neutrino positions and persistently bright portions of the Fermi gamma-ray sky. This possible correlation should be readily testable using eight years of further data already collected by IceCube. We are currently working with Astrophysical Multimessenger Observatory Network (AMON) partner facilities to generate low-latency $\nu + \gamma$ alerts from Fermi-LAT gamma-ray and IceCube and ANTARES neutrino data and distribute these in real time to AMON follow-up partners.

Key words: BL Lacertae objects: general – cosmic rays – gamma-ray burst: general – gamma rays: general – neutrinos

1. Introduction

The IceCube Collaboration has detected the first high-energy neutrinos of cosmic origin (Aartsen et al. 2013a, 2013b). Unlike the atmospheric neutrinos that dominate the observed events at lower energies, the cosmic neutrinos have a harder spectrum, with a current best-fit neutrino power-law index of $\Gamma_{\nu}=-2.19$ (IceCube Collaboration et al. 2017a). The sky distribution of high-likelihood cosmic neutrinos is consistent with isotropy, and indeed, no high-confidence counterparts have been identified for any of these neutrinos (Aartsen et al. 2014, 2017a); however, we note the recent suggestive coincidence between the "extremely high-energy" muon neutrino IceCube-170922A (Kopper et al. 2017) and a bright and extended GeV-flaring episode of the blazar TXS 0506 + 056 (Tanaka et al. 2017).

In addition to blazars, possible cosmic neutrino source populations include star-forming and starburst galaxies, galaxy groups and clusters, other types of active galactic nuclei, supernovae, and gamma-ray bursts (GRBs; see Murase 2015 for a recent review).

One possible approach to revealing the nature of the source population(s) is to take advantage of the likely greater number of cosmic neutrinos that must exist within the IceCube data set at lower energies. For example, using the most recent power-law index and normalization estimates

(IceCube Collaboration et al. 2017a) and integrating down to $\varepsilon_{\nu} \approx 1\,\mathrm{TeV}$ using the facility's decl.- and energy-dependent effective area (Aartsen et al. 2014), we find that IceCube should be detecting $r_{\mathrm{cosmic}} \approx 120$ neutrinos of cosmic origin per year, all-sky, below the $\varepsilon_{\nu} \approx 60\,\mathrm{TeV}$ threshold for individual likely cosmic events (e.g., those selected as IceCube high-energy starting events). If the cosmic neutrino spectrum softens (or becomes dominated by a distinct, softer component) within $1\,\mathrm{TeV} \lesssim \varepsilon_{\nu} \lesssim 60\,\mathrm{TeV}$, then the number of cosmic neutrinos in this range could be substantially greater. However, since these lower energy cosmic neutrinos are individually indistinguishable from the atmospheric neutrino background, some strategy must be employed to identify them before they can be used to study their sources.

One such strategy is illustrated by the IceCube Collaboration's all-sky and catalog-based point-source searches (Aartsen et al. 2014, 2017a; IceCube Collaboration et al. 2017b). These strategies are likely to be optimal in cases where the neutrino sources are persistent, roughly constant, and drawn (respectively) from either unknown or known/anticipated source populations.

Alternatively, for transient or highly variable source populations, we can take advantage of the neutrino timing and localization to attempt to identify electromagnetic or other non-neutrino counterparts. Any such discovery would have immediate implications for the nature of the sources, whether

² Center for Particle & Gravitational Astrophysics, Institute for Gravitation and the Cosmos, Pennsylvania State University, University Park, PA 16802, USA
³ Department of Astronomy & Astrophysics, Pennsylvania State University, University Park, PA 16802, USA

⁴ Center for Theoretical & Observational Cosmology, Institute for Gravitation and the Cosmos, Pennsylvania State University, University Park, PA 16802, USA Received 2018 February 22; revised 2018 July 2; accepted 2018 July 2; published 2018 August 10

or not a host galaxy or long-lived counterpart could also be identified.

As reviewed by Murase (2015), numerous theoretical models predict the co-production of cosmic neutrinos with prompt and luminous electromagnetic signals. In most such models, protons or other nuclei are accelerated to high energies, often in relativistic jets. Interactions of these accelerated particles with ambient matter or radiation yield copious quantities of pions, with gamma rays resulting from decay of the π^0 component, and neutrinos from decays of the co-produced π^\pm . For example, GRBs were long considered potential sources of jointly detected high-energy neutrinos and gamma rays (e.g., Waxman & Bahcall 1997; Bustamante et al. 2015; Mészáros 2015). Although GRBs are now ruled out as the dominant source of IceCube cosmic neutrinos by coincidence studies (Aartsen et al. 2015a), it remains possible that GRBs supply a fraction of the cosmic neutrinos.

Particular sub-classes of GRBs including "choked jet" events could still provide a partial or even dominant contribution to the cosmic neutrinos (Murase & Ioka 2013; Senno et al. 2016; Tamborra & Ando 2016). Other promising neutrino + gammaray ($\nu + \gamma$) transients include luminous supernovae (Murase et al. 2011), blazar flares (e.g., Dermer et al. 2014; Gao et al. 2017), and tidal disruption events (e.g., Dai & Fang 2017; Lunardini & Winter 2017; Senno et al. 2017).

In this context, the *Fermi* satellite's Large Area Telescope (LAT; Atwood et al. 2009) offers a highly complementary data set for cross-reference with IceCube neutrino detections. Operating efficiently over the 100 MeV $\lesssim \varepsilon_\gamma \lesssim$ 300 GeV energy range, the LAT provides instantaneous coverage of roughly 20% of the sky and regular full-sky coverage (under normal operations) every three hours. Its energy range, angular and energy resolution, low background, and sensitivity yield a high-purity sample of high-energy photons that is almost immediately available (median delay of 5 hr) for real-time cross-correlation with IceCube neutrinos.

The high suitability of the Fermi-LAT and IceCube neutrino data sets for joint analysis prompted our previous archival search for subthreshold neutrino + gamma-ray $(\nu + \gamma)$ emitting sources in the IceCube 40-string (hereafter IC 40) public neutrino data set (Keivani et al. 2015). This work, carried out under the auspices of the Astrophysical Multimessenger Observatory Network (AMON⁵; Smith et al. 2013; Cowen et al. 2016), calculated pseudo-likelihoods for all candidate $\nu + \gamma$ pairs and compared the cumulative distribution of this test statistic to a null distribution derived from scrambled data sets (using the Anderson-Darling test; Scholz & Stephens 1987). The sensitivity of the analysis was calibrated via signal injection, allowing a rough mapping of Anderson–Darling *p*-value to the number of injected pairs. While the observed test statistic distribution and the p-value of 4% versus the null distribution were consistent with the presence of ≈70 signal pairs out of 2138 observed coincidences, subsequent vetting tests provided no reason to suspect the presence of a cosmic signal.

The present work can be considered, in part, a continuation and extension of this earlier investigation. First, we revisit the IC 40 analysis using the new *Fermi* Pass 8 reconstruction and extend the analysis to the IceCube public 59-string data set (hereafter IC 59), which covers both northern and southern

hemispheres. Second, we extend the previous test statistic to incorporate the possibility of single neutrino + multiple gamma-ray coincidences, which provides an unbounded statistic suitable for identification of individual high-significance events. Finally, we divided the *Fermi* bandpass into three energy ranges in our background calculations, which we expect will improve the sensitivity of the analysis for relatively hard-spectrum transients.

The paper is organized as follows. Details of the data sets are provided in Section 2, while our statistical approach and signal-injection studies are discussed in Section 3. Unscrambling of the neutrino data sets and results are presented in Section 4, while Section 5 provides our conclusions, including suggestions for future work.

2. Data Sets

This analysis was performed using available IceCube and *Fermi*-LAT public data over the period of temporal overlap between the two observatories. The relevant *Fermi* data were the Pass 8 photon reconstructions available from the LAT FTP server. These photon events were filtered using the Fermi Science Tools, keeping only photons with a zenith angle smaller than 90°, energies between 100 MeV and 300 GeV, detected during good time intervals provided in the LAT satellite files.

The point-spread function (PSF) of the LAT is given by a double King function with the parameters depending on the photon energy, conversion type, and incident angle with respect to the LAT boresight (Ackermann et al. 2013). At lower energies (hundreds of MeV), the angular uncertainty can be several degrees, especially for off-axis photons. At $\varepsilon_{\gamma} > 1$ GeV the average uncertainty drops below 1°, and at $\varepsilon_{\gamma} \gtrsim 100$ GeV, angular uncertainties are better than 0°.1.

Public data from the 40-string (IC 40⁸) and 59-string (IC 59⁹) configurations of IceCube were used (Abbasi et al. 2011; Aartsen et al. 2013c). IC 40 ran from 2008 April to 2009 May and contains 12,876 neutrinos over the northern hemisphere. This corresponds to weeks 9 to 50 of the *Fermi* mission, which has public data available from 4 August 2008. Applying our cuts to the *Fermi* data yield 7.2 million northern-hemisphere photons during IC 40, and reduces the IC 40 neutrino data set to 8871 events over the approximately nine-month period of joint operations. IC 59 ran from 2009 May to 2010 May and contains 107,569 neutrino events; this period corresponds to weeks 50–104 of the *Fermi* mission and yields 19.4 million photon events passing our cuts. Figure 1 shows neutrino sky maps for IC 40 and IC 59 in equatorial coordinates.

We adopt a Gaussian form for the IceCube PSF. For IC 40, the angular uncertainty for each neutrino is set at 0°.7 (Aartsen et al. 2014). Angular uncertainties are provided for the IC 59 events and we use the reported angular uncertainty for each event.

A healpix (Górski et al. 2005) map of resolution 8 (NSide = 256, mean spacing of $0^{\circ}23$) was constructed using the entire *Fermi* data set (weeks 9 to 495 at the time of creation)

⁵ AMON website: http://www.amon.psu.edu/.

⁶ LAT data located at ftp://legacy.gsfc.nasa.gov/fermi/data/lat/weekly/photon/.

Fermi satellite files located at ftp://legacy.gsfc.nasa.gov/fermi/data/lat/weekly/spacecraft/.

⁸ IC 40 data available at http://icecube.wisc.edu/science/data/ic40.

⁹ IC 59 data available at http://icecube.wisc.edu/science/data/IC59-point-source.

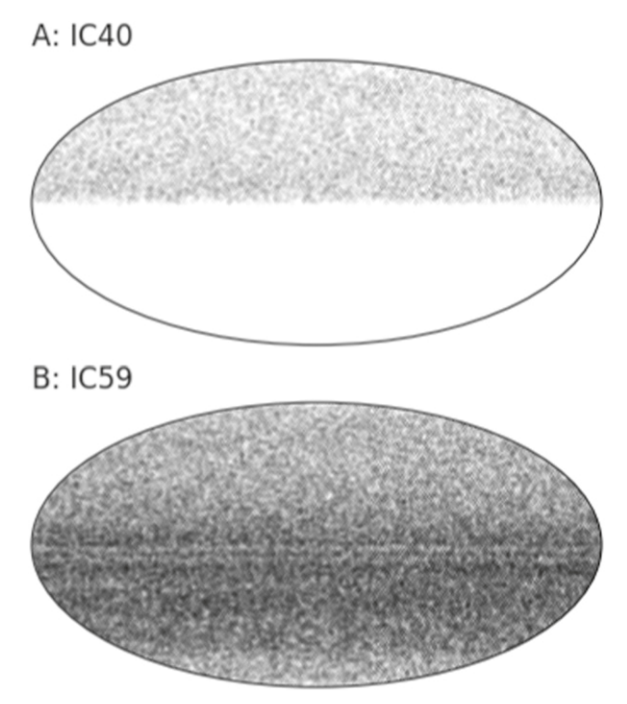


Figure 1. Neutrino sky positions from IC 40 and IC 59. No cosmic structure nor significant point-source detections have been reported from these data (Abbasi et al. 2011; Aartsen et al. 2013c).

with the same photon selection criteria used for IC 40 and IC 59. Using the HEASoft (NASA High Energy Astrophysics Science Archive Research Center (Heasarc), 2014) software, events were binned into three logarithmically uniform energy bins. Each energy bin was then further binned into a healpix map, with the live time calculated via a Monte Carlo simulation. Dividing the counts map by the live time map produced the *Fermi* exposure map. Zero-valued (low-exposure) pixels were replaced by the average of the nearest neighbor pixels. Our three resulting all-sky *Fermi* maps are shown in Figure 2. Due to the additional reconstruction uncertainty in the *Fermi* PSF for high-inclination events (inclination angle greater than 60°), three additional maps were generated by further averaging all pixels with their nearest neighbors.

3. Methods

3.1. Significance Calculation

Our analysis begins by filtering for coincidences between an individual neutrino event and all photons within 5° angular separation and $\pm 100\,\mathrm{s}$ arrival time, as per Keivani et al. (2015). The angular acceptance cut corresponds approximately to the maximum 1σ radial uncertainty for Fermi-LAT photons satisfying our event selection. The temporal acceptance window is chosen to include $\approx\!90\%$ of classical GRBs (Paciesas et al. 1999). For each coincidence, a pseudo-log-likelihood test statistic, λ , is calculated as follows:

$$\lambda = 2 \ln \frac{(P_{\gamma 1}(\mathbf{x}) P_{\gamma 2}(\mathbf{x}) \dots P_{\gamma n}(\mathbf{x})) n! (P_{\nu}(\mathbf{x}))}{B_1(\mathbf{x}, E_1, \theta_1) B_2(\mathbf{x}, E_2, \theta_2) \dots B_n(\mathbf{x}, E_n, \theta_n)},$$
(1)

where n is the number of photons coincident with the neutrino, $P_{\gamma i}(x)$ is the energy-dependent PSF of the LAT at the best-fit position, x, and $P_{\nu}(x)$ is the IceCube PSF at the best-fit position. Both PSFs have units of probability per square

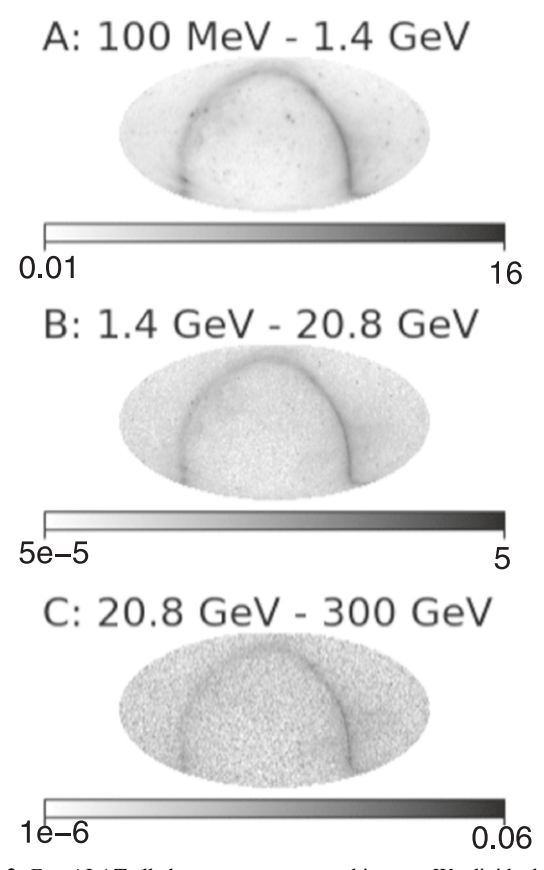


Figure 2. Fermi-LAT all-sky exposure-corrected images. We divide the Fermi data into three bins of equal width in $\log \varepsilon_{\gamma}$ and calculate mission-averaged all-sky images to determine the expected background rate for each photon in the primary analysis. Grayscale intensity units, indicated by the color bars, are photons per 200 seconds per square meter per square degree.

degree. The $B_i(x, E_i, \theta_i)$ are the LAT background terms in units of photons per square meter (approximating the *Fermi* effective area) per 200 s (our temporal window) per square degree for each γ_i , given its energy E_i and inclination angle θ_i . In this metric, larger values of λ indicate a higher likelihood correlated multiplet. This pseudo-log-likelihood statistic is the natural extension of the Keivani et al. (2015) test statistic to multiphoton coincidences, via the Poisson likelihood of generating an n-fold coincidence from background; in the prior approach, each $\nu + \gamma$ coincidence was treated separately.

The best-fit position x is determined as the location of maximal PSF overlap. As the overlap of a double King function with a Gaussian function cannot be solved analytically, the best-fit position is found numerically. For single neutrino + multiple photon coincidences, the event photon multiplicity is determined by optimization: we compare the λ value at maximum multiplicity to that which would result if the photon with the lowest PSF density at the best-fit position were excluded (after recalculating the best-fit position and λ), and iteratively exclude photons until λ no longer increases.

3.2. Analysis Definition

We generate a set of 10,000 Monte Carlo scrambled versions of each of our three data sets in order to characterize their null distributions and define analysis thresholds, prior to performing any analysis of the unscrambled data sets. Our scrambling

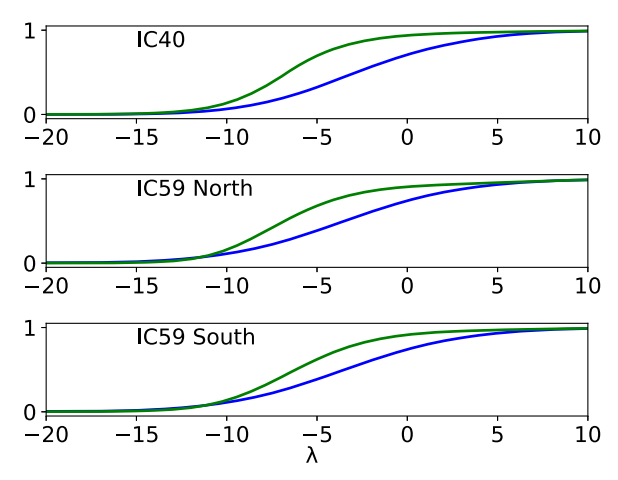


Figure 3. Cumulative distribution of pseudo-log-likelihood (λ) values from null/scrambled (green) and signal-only (blue) realizations of the IC 40 (top), IC 59-North (middle), and IC 59-South (bottom) data sets. Note that the tails of the distributions extend far off of the plots

procedure begins by shuffling the full set of neutrino detections, associating each original neutrino ν_i with another randomly selected neutrino ν_j . Each neutrino ν_i retains its original decl. and angular error and receives the original arrival time of neutrino ν_j , with its new R.A. derived by adjusting the original R.A. for the difference in local sidereal time between the original and new arrival times, the same approach as in Turley et al. (2016). *Fermi*-LAT photons are not scrambled as the LAT data contains known sources and extensive (complex) structure. Coincidence analysis is carried out for each scrambled data set and λ values are calculated for the resulting $\nu + \gamma$ coincidences via Equation (1).

This analysis presents two discovery scenarios. First, since our test statistic λ is unbounded, the null distribution provides us with threshold values, which can be used to identify individually significant coincidences and estimate their false alarm rates. We define two such thresholds, $\lambda_{\times\,10}$, the value exceeded (one or more times) in 1 of 10 scrambled data sets, and $\lambda_{\times\,100}$, the value exceeded in 1 of 100 scrambled data sets. For analyses treating a year of observations, these two thresholds would correspond to events with false alarm rates of 1 decade $^{-1}$ and 1 century $^{-1}$, respectively.

Under this approach (and without accounting for the trials factor, see below), observation of a single event above $\lambda_{\times 100}$, or two events above $\lambda_{\times 10}$, would constitute evidence of joint $\nu + \gamma$ emitting sources, while observation of two events above $\lambda_{\times 100}$ or four events above $\lambda_{\times 10}$ would enable a discovery claim.

In the absence of any individually significant events, there remains the opportunity for discovery of a subthreshold population of $\nu + \gamma$ emitting sources. By design, true cosmic coincidences are biased to higher λ values (Figure 3), and a population containing a sufficient number of such signal events can be distinguished from the null distribution using the Anderson–Darling k-sample test. The k-sample test is used to establish mutual consistency among k observed data sets (k=2 for a two-sample test), testing against the null hypothesis that they are drawn from a single underlying distribution.

Given our choice to make two statistical tests on each of three predefined data sets (IC 40, IC 59-North, and IC 59-South), we apply an $N_{\text{trials}} = 6$ trials penalty to our unscrambled analyses (Section 4.1).

3.3. Signal Injection

To estimate our sensitivity to cosmic $\nu + \gamma$ emitting source populations, we generate signal-like events and inject these into scrambled data sets, comparing the results to the null distribution.

Since we test for γ multiplicity, as part of this process we must adopt a procedure for determining whether each injection is a γ singlet, doublet, or $n_{\gamma} > 2$ multiplet. To determine the appropriate n_{γ} distribution, we assume a population of sources emitting one neutrino, with associated photon fluence distributed according to $N(S \geqslant S_0) \propto S_0^{-3/2}$, where S_0 is a threshold photon fluence and $N(S \geqslant S_0)$ is the number of events observed with fluences greater than or equal to this threshold; we note that an $S_0^{-3/2}$ dependence is expected for source populations of arbitrary luminosity function distributed in Euclidean space.

Adopting a minimum-considered fluence of $S_{\min}=0.001$ photons and inverting this relation, we generate the expectation value for the multiplicity of any event as $\langle n_{\gamma} \rangle = S_{\min} \, u^{-2/3}$, where u is a uniform random variable. We then generate the observed n_{γ} by drawing randomly from the Poisson distribution with expectation value $\langle n_{\gamma} \rangle$. Excluding zero-multiplicity events, we are left with the following n_{γ} distribution: 93% singlet, 4.8% doublet, 1.1% triplet, 0.5% quadruplet, 0.3% quintuplet, 0.2% sextuplet, and 0.1% septuplet (the highest multiplicity we allow). As an aside, we note that this is (approximately) the unique and universal distribution expected to arise in these cases, for extragalactic source populations extending to modest redshift ($z \lesssim 1$) with weak evolution, and thus distributed in near-Euclidean space.

A signal event of photon multiplicity n_{γ} is generated by centering the PSF for n_{γ} LAT photons and an IceCube neutrino at the origin. The neutrino localization uncertainty is drawn from the full set of IceCube neutrino uncertainties, while the inclination angles and conversion types of the photons are drawn from the full set of these distributions within the *Fermi* data set. Photon energies are drawn from a power law with a photon index $\Gamma=-2$. The photons and the neutrino are placed randomly according to their respective PSFs. A random sky position is then chosen as the best-fit position for this coincidence, and a λ value is calculated following the methods of Section 3. Since the λ calculation involves maximizing λ by exclusion of outlying photons, many events end up with some of the injected photons excluded. Cumulative distributions for the null and signal-only distributions are shown in Figure 3.

To calculate the sensitivity of our analysis, we inject an increasing number of signal events $n_{\rm inj}$ into a scrambled (null) distribution and compare the signal-injected and null λ distributions using the Anderson–Darling k-sample test. We carry out 10,000 trials for each selected value of $n_{\rm inj}$ and plot the mean resulting p-value against $n_{\rm inj}$, for each of our data sets, in Figure 4. In this way we estimate the threshold value of $n_{\rm inj}$ that is required to yield a statistically significant deviation from the null distribution for each of the data sets ($n_{\rm inj,1\%}$ and $n_{\rm ini,0.1\%}$ columns in Table 1).

3.4. Analysis Sensitivity and Expectations

Carrying out the scrambled analysis on the IC 40 and IC 59 data produces the null λ distributions shown in Figure 3. Key statistics from these analyses are summarized in Table 1. Most of the simulated events with $\lambda > \lambda_{\times 100}$ in IC 59-North

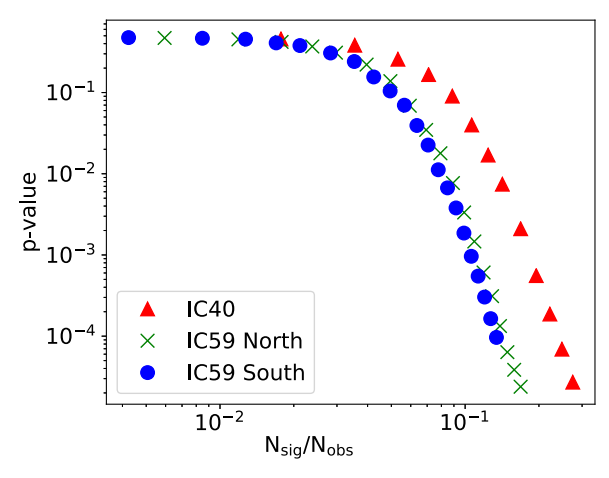


Figure 4. Analysis sensitivity, plotted as Anderson–Darling two-sample *p*-value vs. fraction of coincidences that result from signal events, $n_{\rm inj}/n_{\rm obs}$. Results for IC 40 are plotted in red, IC 59-North in green, and IC 59-South in blue. As expected, these sensitivities scale roughly as $1/\sqrt{n_{\rm obs}}$, so that the larger IC 59-North and IC 59-South data sets provide superior fractional sensitivity than IC 40.

scrambled runs result from a scrambled neutrino landing in near coincidence with one of two GRBs detected by the LAT during our period of observation. GRB 090902B (Abdo et al. 2009) placed over 200 photons on the LAT, giving a maximum $\lambda=2560.2$ in a 218-photon coincidence. GRB 100414A (Takahashi et al. 2010) placed over 20 photons on the LAT and yields a maximum $\lambda=91.2$ in a 10-photon coincidence. Excluding all coincidences with either of these GRBs would yield a threshold of $\lambda_{\times 100}=35$ for the IC 59-North data, rather than the GRB-inclusive value of $\lambda_{\times 100}=49.0$.

Given the number of signal-like $\nu + \gamma$ required to yield a p < 1% deviation in the Anderson–Darling k-sample test, we estimate our analysis would detect >150 source-like $\nu + \gamma$ coincidences from IC 40 (>13% of the total number of coincidences in IC 40), >440 from IC 59-North (>9%), and >565 from IC 59-South (>9%); see Table 1.

4. Results

4.1. Coincidence Search

Applying our analysis to the three unscrambled neutrino data sets yields the results summarized in Table 1. Figures 5 and 6 show the λ distributions for the unscrambled data for IC 40, IC 59-North, and IC 59-South, along with the null distributions, and distributions for signal injections yielding p-values from the Anderson–Darling test of 1% and 0.1%, respectively. All distributions are normalized to the number of coincidences $n_{\nu+\gamma}$ observed in the unscrambled data. No λ values were detected above the $\lambda_{\times 10}$ threshold in any of the analyses. Notably, as seen in Figure 6, the IC 59-North and IC 59-South data show an excess of lower λ values by comparison to the null distributions, unlike the excess of higher λ values expected from a signal population.

Given our six trials, a minimum observed single-trial p=3.8% corresponds to a trials-corrected value of $p_{\rm post}=20.7\%$, which is not significant. However, the similar scale and shape of the residual patterns for IC 59-North and IC 59-South lead us to seek out possible causes of these residual patterns. To illustrate this point, combining p-values from these two data sets (our most sensitive) by Fisher's method gives a

joint p = 3.9% (single trial) as the probability of generating two such large deviations by random chance.

We note that we have not conceived of any way for systematic effects to generate the IC 59 residuals and low *p*-values, simply because any errors or simplifications in the analysis (which certainly exist) are replicated across all scrambled data sets. Rather, the only way to generate these effects (if they are not due to random statistical fluctuation) is via spatio-temporal correlation of neutrinos and gamma rays. Such correlation would imply either cosmic sources, or at a minimum, correlated emission (e.g., enhancement toward the Galactic plane or Supergalactic plane) and hence, require structure in the neutrino sky, which has not previously been observed.

We divide our further explorations into two approaches: first (Section 4.2), we further vet the IC 59 data against our original hypothesis, to test for any evidence that short-duration ($\delta t < 100 \, \mathrm{s}$) $\nu + \gamma$ transients are really present in the data. Second (Section 4.3), we test for longer-duration $\nu + \gamma$ spatiotemporal correlations that might have an effect on our original analysis.

4.2. IC 59 Vetting

We vet the IC 59 data sets to evaluate whether the low p-values and systematic trends in the residual λ distributions that we observe could be due to $\nu + \gamma$ transient sources, as per our original hypothesis, but below the sensitivity of those analyses. We exclude the IC 40 data set from these tests as it is less sensitive to the presence of cosmic sources (see Figure 4 and Section 3.4).

Specifically, we check for systematic trends or anomalies in the spatial and temporal distributions of the neutrino-coincident photons that might account for the unexpected deviation to lower λ values. We test separately for deviations in the distributions of the photons' angular and temporal separations from their coincident neutrino, for IC 59-North and IC 59-South.

With regards to the angular separation distributions, we note that a systematic underestimation of IceCube neutrino localization uncertainties might cause suppressed λ values relative to simulations, due to the P_{ν} term in the pseudo-likelihood. In a similar vein, even if all neutrino and gammaray localization uncertainties are accurately characterized, a systematically softer spectrum for cosmic $\nu + \gamma$ sources $(\Gamma < -2)$ would suppress λ values via the $P_{\gamma i}$ terms in the pseudo-likelihood, since higher-energy LAT photons are better localized.

We construct five-bin histograms of the angular separations of all neutrino-associated photons, with bin boundaries chosen to make the null distribution approximately flat (equal numbers of photons in each bin). We then calculate the χ^2 statistic for the unscrambled data compared to the (flat) null distribution.

Figure 7 (note zero-suppressed y axis) presents our results. Observed IC 59-North angular separations are consistent with the (flat) null distribution, exhibiting $\chi^2=8.238$ for 4 degrees of freedom (p=14.3%). IC 59-South angular separations, by contrast, show a substantial deficit in the bin at $\delta\theta\approx3^\circ$ (and modest excesses in the bins to either side), which results in $\chi^2=11.502$ for 4 degrees of freedom, giving p=4.2%. While this deviation is moderately surprising, the absence of any systematic trend to low or high separations suggests it is

Table 1
Coincidence Search Results

		Thresholds				Observed		
Data Set	$\langle n_{ u+\gamma} angle$	$\lambda_{\times 10}$	$\lambda_{\! imes 100}$	$n_{ m inj,1\%}$	$n_{ m inj,0.1\%}$	$\overline{n_{\nu+\gamma}}$	$\lambda_{ ext{max}}$	p_{A-D}
IC 40	1090 ± 30	23.9	27.2	150	210	1128	20.3	63%
IC 59-North	4970 ± 65	26.5	49.0	440	570	5046	17.8	16.8%
IC 59-South	7072 ± 76	26.8	31.5	565	740	7080	24.4	3.8%

Note. $\langle n_{\nu+\gamma} \rangle$ is the expected number of neutrinos observed in coincidence with one or more gamma rays, as derived from 10,000 Monte Carlo scrambled realizations of each data set. $\lambda_{\times 10}$ and $\lambda_{\times 100}$ are the thresholds above which a coincidence is only observed once per 10 or 100 scrambled data sets, respectively. $n_{\text{inj},1\%}$ and $n_{\text{inj},0.1\%}$ are the number of injected signal events required in simulations to give an Anderson–Darling test statistic of p < 1% and p < 0.1%, respectively, by comparison to the null distributions for each data set. $n_{\nu+\gamma}$ is the number of neutrinos observed in coincidence with one or more gamma rays in the unscrambled data, λ_{max} is the maximum observed λ for each data set, and $p_{\text{A}-\text{D}}$ is the value of the Anderson–Darling test statistic from comparison of the observed λ distribution to its associated null distribution.

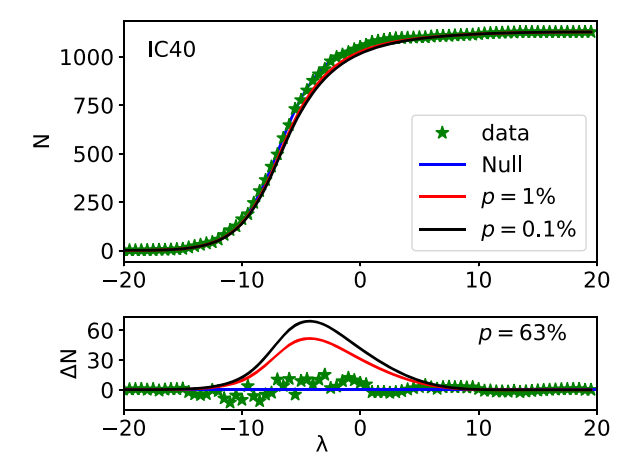


Figure 5. Cumulative and residual test statistic (λ) distributions for IC 40 ($n_{\nu+\gamma}=1128$). Upper panel: cumulative IC 40 λ distributions for unscrambled data (green stars), scrambled data/null distribution (blue line), and signal injections yielding p=1% (red line) and p=0.1% (black line). Lower panel: residuals, plotted as null minus alternative, for IC 40 data (green stars) and the two signal-injection distributions (red and black lines).

likely not responsible for the observed deviation in the λ distribution.

Here we note that a systematic trend to small angular separations would suggest the presence of $\nu + \gamma$ sources as per our test hypothesis, while a systematic trend to large angular separations would suggest the presence of $\nu + \gamma$ sources with underestimated localization uncertainties or soft gamma-ray spectra. Neither such trend is observed.

We execute a similar analysis of the temporal separations of coincident photons. In contrast to the angular separations, which are incorporated into our pseudo-likelihood calculation, temporal separations are not considered (apart from the predefined acceptance window), so this analysis serves as an independent test of our original hypothesis. For purposes of trials correction of any subsequent statistics, we therefore add two trials, giving $N_{\rm trials} = 8$.

Figure 8 (note zero-suppressed y axis) shows our results for temporal separations data in the two IC 59 data sets. Neither data set shows evidence for deviation from the expected flat distribution (illustrated using scrambled data sets), with χ^2 -derived p-values of p=73% for IC 59-North and p=53% for IC 59-South.

Examining the angular and timing separations of the neutrinos and coincident photons at higher resolution thus

provides no support for the presence of short-duration $(\delta t \lesssim 100~{\rm s})~\nu + \gamma$ emitting cosmic sources as conceived in our original hypothesis. Since these are not seen, we move on to examine alternative models that might generate $\nu + \gamma$ spatio-temporal correlations in the data.

4.3. Tests for $\nu + \gamma$ Correlation

We carry out two tests for spatio-temporal correlations between the neutrino and gamma-ray data sets beyond our original ± 100 s temporal acceptance window.

First, a correlation between neutrino and photon positions on the sky, without any temporal correlation (i.e., in steady state) could suppress λ values relative to the null hypothesis, due to the B_i gamma-ray background terms in our pseudo-likelihood (Equation (1)).

To test for positional correlation, we first construct a single *Fermi* background map covering the full energy range. We then measure the background value at the location of every IceCube neutrino in unscrambled data and compute the average photon background for the neutrino map. This average is then compared to the average backgrounds from each of the 10,000 scrambled data sets. The scrambled data sets give an average background of $(1.90 \pm 0.015) \times 10^{-2}$ photons deg⁻² m⁻² per 200 s for IC 59-North and $(2.40 \pm 0.022) \times 10^{-2}$ photons deg⁻² m⁻² per 200 s for IC 59-South. The observed average backgrounds (in the same units) from unscrambled data are 1.91×10^{-2} (+0.58 σ ; p = 28.1%) for IC 59-North and 2.44×10^{-2} (+1.67 σ ; p = 4.7%) for IC 59-South. These observed values are presented in the context of the distributions from scrambled data in Figure 9.

This analysis is not an independent test for the presence of $\nu+\gamma$ sources, but rather, an attempt to identify an underlying reason for the trend in λ residuals seen in Section 4.1. Since the p-value for the separate analyses, as well as their combination (p=7.0% by Fisher's method), are within a factor of two of the p-values from the corresponding λ distribution tests, this provides reason to interpret the latter result as (at least in part) due to the observed tendency of IC 59 neutrinos to land on systematically brighter regions of the gamma-ray sky. We reiterate that while this tendency is present in the data, it is not sufficiently strong (in a statistical sense) to support an evidence claim.

As an alternative approach, we check for correlated $\nu+\gamma$ variability on timescales beyond our predefined $\pm 100\,\mathrm{s}$ temporal window but shorter than the full extent of the *Fermi* mission. To this end, for each neutrino in our scrambled IC 59 data sets, we use the total *Fermi* mission background map to

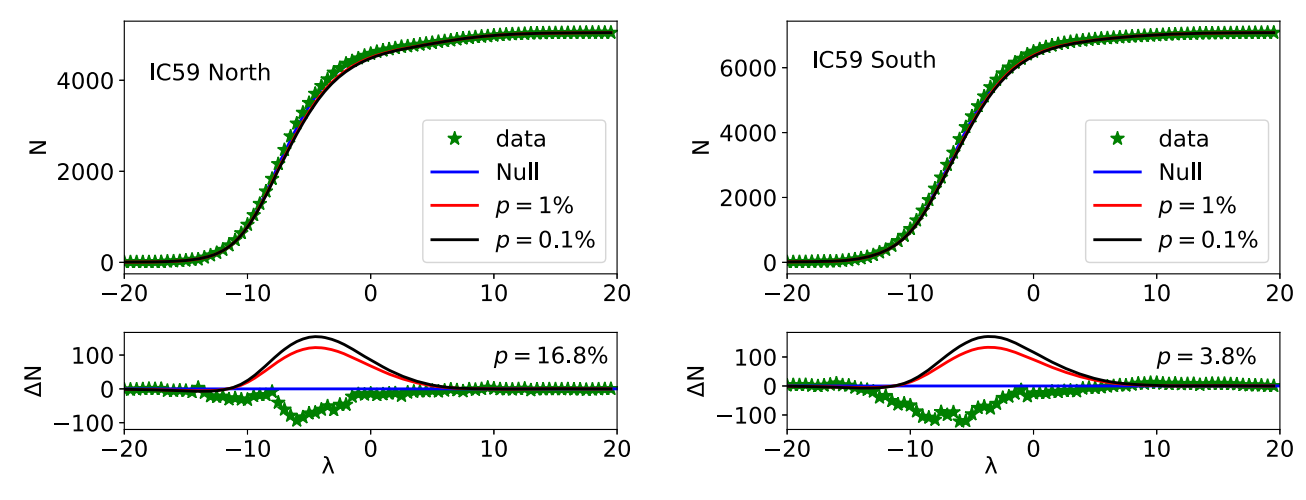


Figure 6. Cumulative and residual test statistic (λ) distributions for IC 59-North (left) and IC 59-South (right). Left: cumulative (upper panel) and residual (lower panel) λ distributions for IC 59-North ($n_{\nu+\gamma}=5046$), including unscrambled data (green stars), scrambled data/null distribution (blue line), and signal injections yielding p=1% (red line) and p=0.1% (black line). Residuals are plotted as null minus alternative. Right: cumulative (upper panel) and residual (lower panel) λ distributions for IC 59-South ($n_{\nu+\gamma}=7080$), including unscrambled data (green stars), scrambled data/null distribution (blue line), and signal injections yielding p=1% (red line) and p=0.1% (black line). A similar and unexpected pattern is noted in the residual λ distributions for the IC 59-North and IC 59-South data sets.

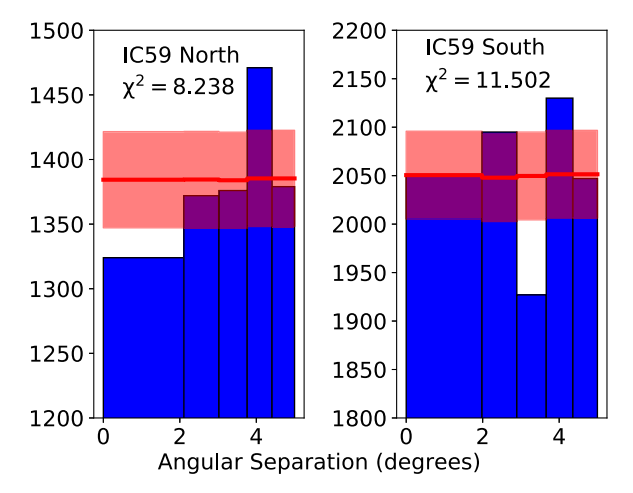


Figure 7. IC 59 $\nu+\gamma$ angular separations. We test the observed angular separation distribution for neutrino-coincident photons (blue histograms) in IC 59-North (left) and IC 59-South (right) against the null distribution (red), which is approximately flat by construction (via choice of histogram bin boundaries). The $\pm 1\sigma$ ranges expected for a single data set on the basis of Poisson uncertainties are indicated as the red range; note zero-suppressed y axis.

calculate the number of photons expected to arrive within 5° of the neutrino position and $\pm 50,000\,\mathrm{s}$ of the neutrino arrival time (excluding the $\pm 100\,\mathrm{s}$ window used in the original analysis). We then count the number of photons arriving within this spatio-temporal window (again, summing results across our three *Fermi* energy bands). For each neutrino, the observed number of photons within the extended temporal window is expressed as a Poisson fluctuation on the number expected by normalizing against the full *Fermi* mission. We quantify the magnitude of this fluctuation as a *p*-value and find the equivalent number of σ for a Gaussian distribution, yielding a statistic that we call the local excursion *E* for that neutrino. The distribution of excursions from all neutrinos in unscrambled data can then be compared to expectations from scrambled data.

We perform the same two tests that we developed in our primary analysis above. First, we check for individual events that exhibit an unusually large excursion, exceeding either the 1 in $10 \ (E_{\times 10})$ or 1 in $100 \ (E_{\times 100})$ thresholds from scrambled data.

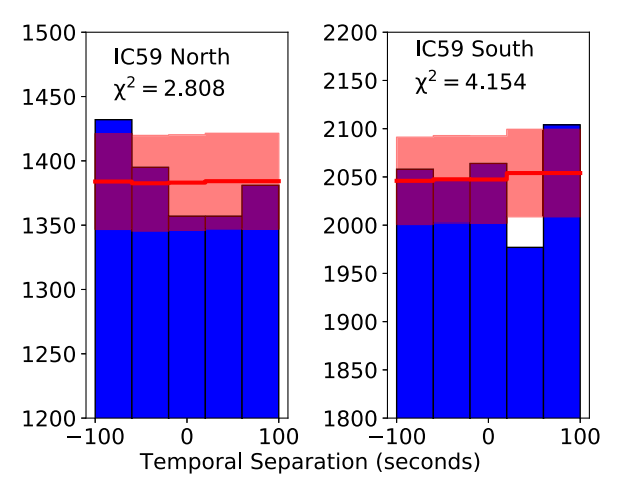


Figure 8. IC 59 $\nu + \gamma$ temporal separations. We test the observed temporal separation distribution for neutrino-coincident photons (blue histograms) in IC 59-North (left) and IC 59-South (right) against the approximately flat null distribution (red). The $\pm 1\sigma$ ranges expected for a single data set on the basis of Poisson uncertainties are indicated by the red range; note zero-suppressed ν axis.

Second, we compare the excursion distribution from unscrambled data to the null distribution from scrambled data using the Anderson–Darling k-sample test. Since this analysis involves two further independent tests of the two data sets, we add four trials for purposes of trial correction of any subsequent statistics, giving $N_{\text{trials}} = 12$.

Excursion thresholds for the two data sets are $E_{\times 10} = 614$ and $E_{\times 100} = 1285$ for IC 59-North, and $E_{\times 10} = 333$ and $E_{\times 100} = 1075$ for IC 59-South. As in our primary analysis, the highest-excursion events in the scrambled data are due to the two GRBs observed in the IC 59-North data. Excluding these GRBs would give excursion thresholds of $E_{\times 10} = 575$ and $E_{\times 100} = 1102$ for IC 59-North.

Analyzing the unscrambled IC 59 data sets reveals no excursions above the $E_{\times 10}$ threshold for either data set. Performing the Anderson–Darling test on the null and unscrambled distributions yields p=55% for IC 59-North and p=62% for IC 59-South. We therefore see no evidence

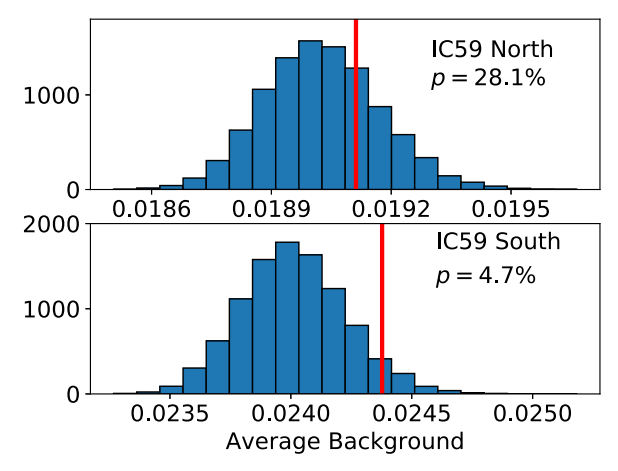


Figure 9. Average *Fermi* gamma-ray background rates at the positions of IC 59-North (upper panel) and IC 59-South (lower panel) neutrinos. In each panel, the histogram shows the distribution from 10,000 Monte Carlo scrambled data sets, while the red line marks the observed background rate for unscrambled data. Background rates are expressed in units of photons $m^{-2} deg^{-2}$. Observed neutrino positions show a mild statistical preference for higher-background regions of the *Fermi* gamma-ray sky, with a joint *p*-value for the two hemispheres of p = 7.0% by Fisher's method.

for spatio-temporal correlation of the neutrinos and *Fermi* gamma rays on the \sim 0.5 day timescale that we probed.

We conclude that the observed tendency of IC 59 neutrinos to arrive from brighter portions of the *Fermi* gamma-ray sky, while potentially due to a statistical fluctuation (single-trial p=7.0% for the two hemispheres combined), is both intriguing in its own right and likely explains the systematic trends in λ residuals against scrambled data sets observed for both hemispheres in our original analysis (single-trial p=3.9% for the two hemispheres combined). While this p-value cannot support an evidence or discovery claim in the context of our multistage analysis, it nonetheless points the way to interesting future analyses that could make use of eight further years of IceCube data from the 79-string and full-strength (86-string) arrays.

In particular, we note that it is a low-level (single neutrino) correlation between the neutrino and gamma-ray skies that has prompted current interest in the blazar TXS 0506 + 056 and its possible neutrino IceCube-170922A (Tanaka et al. 2017).

5. Conclusions

We have carried out an archival coincidence search for neutrino + gamma-ray emitting transients using publicly available Fermi-LAT gamma-ray data and IceCube neutrino data from its 40-string and 59-string runs, incorporating Fermi data from the start of mission in 2008 August through 2010 May. Our search was designed to be capable of identifying $\nu + \gamma$ transients either as individual high-significance singleneutrino events with high gamma-ray multiplicity, or as a population, via statistical comparison of the observed pseudolikelihood distributions to those of uncorrelated (scrambled) data sets.

Using Monte Carlo simulations and signal injection, we demonstrated sensitivity to single-neutrino events of sufficient gamma-ray multiplicity. High-multiplicity gamma-ray clusters have been observed throughout the *Fermi* mission in coincidence with bright LAT-detected GRBs, including two bursts occurring

during our period of study, GRB 090902B (>200 photons; Abdo et al. 2009) and GRB 100414A (>20 photons; Takahashi et al. 2010).

We established sensitivity to subthreshold populations of transient $\nu + \gamma$ sources at the >13% (IC 40), >9% (IC 59-North), and >8% (IC 59-South) level for the three hemispherespecific neutrino data sets we analyzed (p = 1% threshold; Section 3.4). These limits are expressed as the fraction of all neutrinos present in the data sets that are due to $\nu + \gamma$ transient sources ($\delta t < 100 \text{ s}$), according to our assumptions (Section 3.3). Expressed as event rates, the limits correspond to >210 (IC 40), >440 (IC 59-North), and >565 (IC 59-South) gamma-ray associated neutrinos per hemisphere per year. Sensitivity of a joint analysis of the IC 59 data sets was not separately established but can be estimated at >850 gamma-ray associated neutrinos per year all-sky. While these limits are well above the conservative limit of $r_{\text{cosmic}} \gtrsim 120$ neutrinos per year all-sky for the full detector array that we derive on the basis of the $\varepsilon_{\nu} \gtrsim 60 \, {\rm TeV}$ cosmic neutrino spectrum (Section 1), that rate could be substantially larger if the cosmic neutrino spectrum softens significantly within the 1 TeV $\lesssim \varepsilon_{\nu} \lesssim$ 60 TeV range relevant to these data.

Unscrambling the neutrino data, we identify no individual high-significance neutrino + high gamma-multiplicity events and no significant deviations from the null test statistic (λ) distributions. However, we observe a similar and unexpected pattern in the λ residuals from the IC 59-North and IC 59-South analyses, our two more-sensitive data sets, corresponding to a joint p-value of 3.9% (Section 4.1). While granting that these residual patterns may be due to statistical fluctuations, we carried out additional investigations in an attempt to determine the origin of the deviations and whether or not they suggest the presence of $\nu + \gamma$ correlated emission.

We first vetted the IC 59 data for short timescale transients (our original test hypothesis) in two ways, checking for systematic trends in the temporal and spatial separations of the neutrino event and its associated gamma rays. No systematic trends in spatial or temporal separation are evident for either IC 59-North or IC 59-South (Section 4.2).

We then checked for $\nu + \gamma$ spatio-temporal correlations on timescales beyond our original $\pm 100\,\mathrm{s}$ window (Section 4.3). We searched for neutrino-correlated gamma-ray flux excursions within a $\pm 50,000\,\mathrm{s}$ ($\sim 0.5\,\mathrm{day}$) window centered on the neutrino arrival time, finding no evidence for correlated gamma-ray flux excursions on this timescale. Instead, we find a likely correlation (p=7.0%, single trial) of IC 59 neutrino positions with persistently bright portions of the *Fermi* gamma-ray sky.

This interesting and unexpected finding of our search for cosmic $\nu + \gamma$ sources, a possible signature of gamma-ray correlated structure in the high-energy neutrino sky, should be readily testable using eight years of further data already collected by the 79-string and full-strength (86-string) IceCube.

In particular, if blazars are responsible for a non-negligible fraction of the highest-energy cosmic neutrinos, then—given the brightness of the blazar population over the 100 MeV $\lesssim \varepsilon_\gamma \lesssim 300$ GeV LAT bandpass—this would generate correlated structure in lower energy neutrinos. Blazar associations have been proposed for two likely cosmic high-energy neutrinos, IceCube-121204 "Big Bird" and IceCube-170922A, thanks to

their spatio-temporal proximity to flaring episodes of the blazars PKS B1424—418 (Kadler et al. 2016) and TXS 0506 + 056 (Tanaka et al. 2017), respectively. On the other hand, blazar models are strongly constrained by the IceCube *Fermi*-blazar stacking analysis (Aartsen et al. 2017b) and by the absence of detected neutrino point sources (Aartsen et al. 2015b; Murase & Waxman 2018).

In a general sense, some level of correlation between the gamma-ray and neutrino skies is anticipated in models that propose a common origin for the diffuse $\varepsilon_{\nu}\gtrsim 100\,\mathrm{TeV}$ neutrino and $\varepsilon_{\gamma}\lesssim 1\,\mathrm{TeV}$ gamma-ray backgrounds (Murase et al. 2013; Fang & Murase 2018).

Finally, production of some cosmic neutrinos by Galactic sources, whether compact binaries (Abdo et al. 2012; Anchordoqui et al. 2014), TeV unidentified sources or hypernova remnants (Budnik et al. 2008; Fox et al. 2013; Ahlers & Murase 2014), or other source population(s), would naturally lead to correlated structure, given the very prominent Galactic signature in *Fermi* all-sky maps (Figure 2).

Looking ahead, we eagerly anticipate the results of a systematic and comprehensive search for *Fermi* gamma-ray correlated structure in the full IceCube data set. In addition, having demonstrated its effectiveness on archival data, we will be working with IceCube, ANTARES (ANTARES Collaboration 1999), and other partner facilities of the AMON to deploy our neutrino + high gamma-multiplicity search and generate low-latency (delays of ≈ 5 hr) $\nu + \gamma$ alerts from *Fermi*-LAT gamma-ray and IceCube and ANTARES neutrino data. These AMON alerts will be distributed in real time to AMON follow-up partners, prompting rapid-response follow-up observations across the electromagnetic spectrum.

The authors thank Erik Blaufuss and David Thompson for helpful discussions. We gratefully acknowledge support from Penn State's Office of the Senior Vice President for Research, the Eberly College of Science, and the Penn State Institute for Gravitation and the Cosmos. This work was supported in part by the National Science Foundation under grant No. PHY-1708146. K.M. is supported by the Alfred P. Sloan Foundation and by the National Science Foundation under grant No. PHY-1620777.

Software: Astropy (The Astropy Collaboration et al. 2018), Matplotlib (Hunter 2007), HEASoft (NASA High Energy Astrophysics Science Archive Research Center (Heasarc), 2014), HEALPix (Górski et al. 2005), SciPy (Jones et al. 2001).

ORCID iDs

```
C. F. Turley https://orcid.org/0000-0002-9689-8075
D. B. Fox https://orcid.org/0000-0002-3714-672X
A. Keivani https://orcid.org/0000-0001-7197-2788
J. J. DeLaunay https://orcid.org/0000-0001-5229-1995
H. A. Ayala Solares https://orcid.org/0000-0002-2084-5049
K. Murase https://orcid.org/0000-0002-5358-5642
```

References

```
Aartsen, M. G., Abbasi, R., Abdou, Y., et al. 2013a, PhRvL, 111, 021103
Aartsen, M. G., Abbasi, R., Abdou, Y., et al. 2013b, Sci, 342, 1242856
Aartsen, M. G., Abbasi, R., Abdou, Y., et al. 2013c, ApJ, 779, 132
Aartsen, M. G., Abbasi, R., Abdou, Y., et al. 2014, PhRvD, 89, 102004
Aartsen, M. G., Abraham, K., Ackermann, M., et al. 2017a, ApJ, 835, 151
Aartsen, M. G., Abraham, K., Ackermann, M., et al. 2017b, ApJ, 835, 45
Aartsen, M. G., Ackermann, M., Adams, J., et al. 2014, ApJ, 796, 109
Aartsen, M. G., Ackermann, M., Adams, J., et al. 2015a, ApJL, 805, L5
Aartsen, M. G., Ackermann, M., Adams, J., et al. 2015b, APh, 66, 39
Abbasi, R., Abdou, Y., Abu-Zayyad, T., et al. 2011, PhRvD, 84, 082001
Abdo, A. A., Abeysekara, U., Allen, B. T., et al. 2012, ApJ, 753, 159
Abdo, A. A., Ackermann, M., Ajello, M., et al. 2009, ApJL, 706, L138
Ackermann, M., Ajello, M., Allafort, A., et al. 2013, ApJ, 765, 54
Ahlers, M., & Murase, K. 2014, PhRvD, 90, 023010
Anchordoqui, L. A., Goldberg, H., Paul, T. C., da Silva, L. H. M., &
   Vlcek, B. J. 2014, PhRvD, 90, 123010
ANTARES Collaboration 1999, arXiv:astro-ph/9907432
Atwood, W. B., Abdo, A. A., Ackermann, M., et al. 2009, ApJ, 697, 1071
Budnik, R., Katz, B., MacFadyen, A., & Waxman, E. 2008, ApJ, 673, 928
Bustamante, M., Baerwald, P., Murase, K., & Winter, W. 2015, NatCo, 6, 6783
Cowen, D. F., Keivani, A., & Tešić, G. 2016, EPJWC, 116, 10001
Dai, L., & Fang, K. 2017, MNRAS, 469, 1354
Dermer, C. D., Murase, K., & Inoue, Y. 2014, JHEAp, 3, 29
Fang, K., & Murase, K. 2018, NatPh, 14, 396
Fox, D. B., Kashiyama, K., & Mészarós, P. 2013, ApJ, 774, 74
Gao, S., Pohl, M., & Winter, W. 2017, ApJ, 843, 109
Górski, K. M., Hivon, E., Banday, A. J., et al. 2005, ApJ, 622, 759
Hunter, J. D. 2007, CSE, 9, 90
IceCube Collaboration, Aartsen, M. G., Ackermann, M., et al. 2017a,
  arXiv:1710.01191
IceCube Collaboration, Aartsen, M. G., Ackermann, M., et al. 2017b, ApJ,
Jones, E., Oliphant, T., Peterson, P., et al. 2001, SciPy: Open source scientific
  tools for Python, http://www.scipy.org/
Kadler, M., Krauß, F., Mannheim, K., et al. 2016, NatPh, 12, 807
Keivani, A., Fox, D. B., Tešić, G., Cowen, D. F., & Fixelle, J. 2015,
  arXiv:1508.01315
Kopper, C., Blaufuss, E. & IceCube Collaboration 2017, GCN, 1, 21916
Lunardini, C., & Winter, W. 2017, PhRvD, 95, 123001
Mészáros, P. 2015, arXiv:1511.01396
Murase, K. 2015, in AIP Conf. Ser. 1666, XXVI International Conference
  On Neutrino Physics and Astrophysics: Neutrino 2014, ed. E. Kearns &
  G. Feldman (Melville, NY: AIP), 040006
Murase, K., Ahlers, M., & Lacki, B. C. 2013, PhRvD, 88, 121301
Murase, K., & Ioka, K. 2013, PhRvL, 111, 121102
Murase, K., Thompson, T. A., Lacki, B. C., & Beacom, J. F. 2011, PhRvD, 84,
  043003
Murase, K., & Waxman, E. 2016, PhRvD, 94, 103006
Nasa High Energy Astrophysics Science Archive Research Center (Heasarc)
  2014, HEAsoft: Unified Release of FTOOLS and XANADU, Astrophysics
  Source Code Library, ascl:1408.004
Paciesas, W. S., Meegan, C. A., Pendleton, G. N., et al. 1999, ApJS, 122, 465
Scholz, F. W., & Stephens, M. A. 1987, J. Am. Stat. Assoc., 82, 918
Senno, N., Murase, K., & Mészáros, P. 2016, PhRvD, 93, 083003
Senno, N., Murase, K., & Mészáros, P. 2017, ApJ, 838, 3
Smith, M. W. E., Fox, D. B., Cowen, D. F., et al. 2013, APh, 45, 56
Takahashi, H., Ohno, M., & Omodei, N. 2010, GCN, 1, 10594
Tamborra, I., & Ando, S. 2016, PhRvD, 93, 053010
Tanaka, Y. T., Buson, S., & Kocevski, D. 2017, ATel, 10791
The Astropy Collaboration, Price-Whelan, A. M., Sipőcz, B. M., et al. 2018,
  arXiv:1801.02634
Turley, C. F., Fox, D. B., Murase, K., et al. 2016, ApJ, 833, 117
Waxman, E., & Bahcall, J. 1997, PhRvL, 78, 2292
```